Numerical Study on Fluid-Structure Interaction in a Patient-Specific Abdominal Aortic Aneurysm for Evaluating Wall Heterogeneity and Material Model Effects on its Rupture

Y. Mesri[1,2], H. Niazmand[1,2†] and A. Deyranlou[1,2]

[1] Department of Mechanical Engineering, Ferdowsi University of Mashhad, Mashhad, Iran
[2] Research Center for Biomedical Engineering, Ferdowsi University of Mashhad, Mashhad, Iran

†*Corresponding Author Email: niazmand@um.ac.ir*

ABSTRACT

Abdominal Aortic Aneurysm (AAA) is one of the main cardiovascular diseases, which threats human's health while it appears, develops and in crucial cases ruptures and leads to hemorrhage. In the current work, we aim to investigate numerically the transient blood flow in a patient-specific AAA model, while effects of wall compliance is considered by employing the fluid-structure interaction method. The AAA model is reconstructed from acquired CT angiographic data of a patient diagnosed with AAA and an intraluminal thrombus (ILT). For the comparison purposes two different material models, i.e. isotropic and anisotropic are considered. Additionally, to have a better estimation, wall thickness variability is compared with simpler uniform wall thickness model. In this study Navier-Stokes equations along with elastodynamics equation are coupled through Arbitrary Lagrangian-Eulerian formulation method and solved numerically. Findings demonstrate that the isotropic material model with uniform wall thickness significantly underestimates wall stresses as compared to the anisotropic material model with variable wall thickness. Indeed, results emphasize that considering vessel wall as an anisotropic, heterogeneous (variable thickness) structure estimates much higher wall stresses comparing with isotropic, uniform thickness model. Therefore, given realistic vessel wall structure and the fact that the anisotropic, variable wall thickness model predicts higher wall stresses, it could be a more reliable model to give an accurate estimation to physicians to diagnose the stage of a disease and choosing an appropriate therapeutic procedure.

Keywords: Abdominal aortic aneurysm; Fluid-structure interaction; Material model; Wall thickness.

NOMENCLATURE

p	pressure	δ_{ij}	Kronecker delta
$\dot{d}$	local velocity	τ	shear stress
$\ddot{d}$	local acceleration	σ	stress
v	velocity	ε	strain rate
		∇	del operator
μ	dynamic viscosity	ρ	density

1. INTRODUCTION

Clinical evidences show that the rupture risk of abdominal aortic aneurysm (AAA) is positively associated with aneurysm diameter (Lederle *et al*., 2002). The focus of debate for clinical management is in the range of 4cm to 6cm, through which probability of AAA ruptures increases significantly.

However, recent investigations indicate the inadequacy of recommending intervention based solely on this criterion (Grootenboer *et al*., 2009; Vorp, 2007), therefore more researches are necessary (Wassef *et al*., 2007).

Decades of studies on the AAAs have shown that in addition to biological factors (Choke *et al*., 2005), several mechanical factors affect the wall stress

Table 1 Studies over time on the AAAs based on finite element method

Paper	Material model	Wall thickness	ILT material	comments
(Raghavan *et al*., 2000)	Isotropic	Uniform	-	-
(Fillinger *et al*., 2002)	Isotropic	Uniform	-	Stress better than diameter
(Wolters *et al*., 2005)	Isotropic	Uniform	-	Early FSI
(Lu *et al*., 2007)	Isotropic	Uniform	-	-
(Speelman *et al*., 2006)	Isotropic	Uniform	Nonlinear, Isotropic	-
(Scotti *et al*., 2008)	Isotropic	Variable	-	FSI, idealized geometry
(Rodríguez *et al*., 2008)	Anisotropic	Uniform	-	Idealized geometry
(Rissland *et al*., 2008)	Anisotropic	Uniform	Linear	FSI
(Dorfmann *et al*., 2010)	Isotropic	Uniform	-	-
(Maier *et al*., 2010)	Isotropic	Uniform	Nonlinear, Isotropic	-
(Gasser *et al*., 2010)	Isotropic	Variable	Variable stiffness	-
(Raut *et al*., 2013)	Isotropic	Variable	-	-
(Xenos *et al*., 2015)	Anisotropic	Uniform	Linear	FSI

including flow regime (Dua and Dalman, 2010; Scotti and Finol, 2007), vessel geometry (Di Martino and Vorp, 2003; Kleinstreuer and Li, 2006; Li and Kleinstreuer, 2006; Rodríguez *et al*., 2008; Sacks *et al*., 1999; Scotti *et al*., 2005; Venkatasubramaniam *et al*., 2004; Vorp *et al*., 1998), and mechanical properties of the arterial wall (Di Martino and Vorp, 2003; Polzer *et al*., 2013; Raghavan and Vorp, 2000; Rodríguez *et al*., 2008; Vorp, 2007).

Over the past few years, many endeavors have been done for modeling AAAs in order to correlate the risk of AAA rupture and its mechanical characteristics. Recent investigations suggest that peak wall stress predicts the risk of rupture better than the maximal diameter (Fillinger *et al*., 2003; Fillinger *et al*., 2002; Truijers *et al*., 2007; Venkatasubramaniam *et al*., 2004). Indeed they demonstrate that the aneurysm rupture occurs as physiological forces exceed the wall strength of aneurysmal sac. It is now well accepted that the wall stress is an important index in the assessment of AAA rupture. Furthermore, in large arteries, the deformability of the vessel wall greatly affects blood hemodynamics, thus for a more accurate simulation, fluid-structure interaction (FSI) analysis must be taken into account (Rissland *et al*., 2008; Scotti and Finol, 2007; Vorp, 2007; Wolters *et al*., 2005).

One popular approach for stress analysis of AAA is to use patient-specific models that are constructed from clinical images (Di Martino *et al*., 2001; Dorfmann *et al*., 2010; Doyle *et al*., 2010; Raut *et al*., 2013; Rissland *et al*., 2008; Speelman *et al*., 2006; Wolters *et al*., 2005; Xenos *et al*., 2010). Clearly, the shape of an AAA and the thickness of the arterial wall are the major factor in determination of the arterial wall stress distribution

(Raut *et al*., 2013; Scotti *et al*., 2008). Hence, the wall thickness by itself is an important indicator, which contributes significantly in the mechanical response of AAA toward peripheral forces.

In addition to the wall thickness, nonlinear behavior of AAA wall, and the spatial distribution of constituent materials are considered important factors for robust FSI simulations of AAA and more accurate analysis of its rupture risk (Rissland *et al*., 2008; Xenos *et al*., 2015).

The accuracy of AAA FSI analysis has been developed considerably over time. Early studies generally used idealized AAA geometrical models with a uniform wall thickness (UWT) and isotropic behavior for the wall material. Recent FSI works have included more real characteristics of AAAs such as patient-specific geometries, variable wall thickness (VWT), and anisotropic wall material. Table 1 demonstrates recent studies reviewed by Humphrey and Holzapfel (2012) and those added in the present work.

Table 1 indicates that in most of the previous FSI studies wall thickness variability were ignored. Also, those studies that were employed VWT model, in some cases FSI stress analysis were neglected (Gasser *et al*., 2010; Raut *et al*., 2013), and in other cases idealized geometrical model or isotropic material for the wall were employed (Gasser *et al*., 2010; Raut *et al*., 2013; Scotti *et al*., 2008). Furthermore, most of these studies ignored the presence of intraluminal thrombus, while the cumulative effects of wall heterogeneity and material model have been frequently disregarded.

In the present study, a new three-dimensional patient-specific geometrical model of AAA is selected for implementing FSI simulation. Generally, current work aims to study effects of

wall thickness variability (wall heterogeneity), material models and presence of ILT. In the solid domain, the arterial wall without and with variable thickness are selected to compare wall heterogeneity effects. Moreover, two different isotropic and anisotropic material models are employed for investigating the material model effects. Additionally, a non-linear ILT material is considered in the simulations which presents a more realistic behavior in comparison with the linear material model used in the previous study by Rissland *et al.* (2008).

2. AAA RECONSTRUCTION

A three dimensional patient-specific AAA model was constructed for this study based on the CT images of an unruptured AAA including anatomical details of the lumen and ILT from a 61-years-old male patient suffered by AAA. This study was approved by the internal review boards of Ferdowsi University of Mashhad.

Boundaries of the reconstructions for the AAA geometrical model were established from inferior to the renal arteries until 35 mm distal to the iliac bifurcation. The parallel CT images were translated into 3D images using Mimics (Mimics, Materialise, Leuven, Belgium). Mimics allows the user to reconstruct the multidomain AAA geometry with a lumen and intraluminal thrombus. Then the ILT was subtracted from the lumen. Fig.1 shows the AAA geometrical model with luminal volume and ILT.
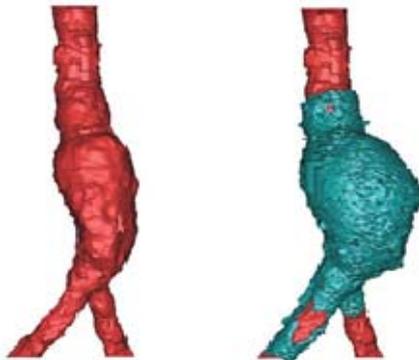

Fig. 1. Initial geometrical model reconstructed from CT angiographic scans. The red color represents the blood domain and the green color represents the ILT.

Afterward, the model was exported to a 3D CAD software, Solidworks. A splitting procedure was performed in Solidworks to create a smooth exterior volume. A constant wall thickness of 1.5 mm was added to the exterior surfaces for the UWT model, while VWT model is constructed based on the study of Scotti *et al.* (2008). The thickness of VWT model varies from 0.5mm to 1.5mm based on the constant wall volume assumption in which the arterial thickness changes in accordance with the distance from arterial centerline. The resulting body

smoothed and imported into ADINA v8.4 software package (Watertown, MA). Fig.2a represents the luminal volume as the fluid domain and Fig. 2b represents the solid domain including the ILT and arterial wall.
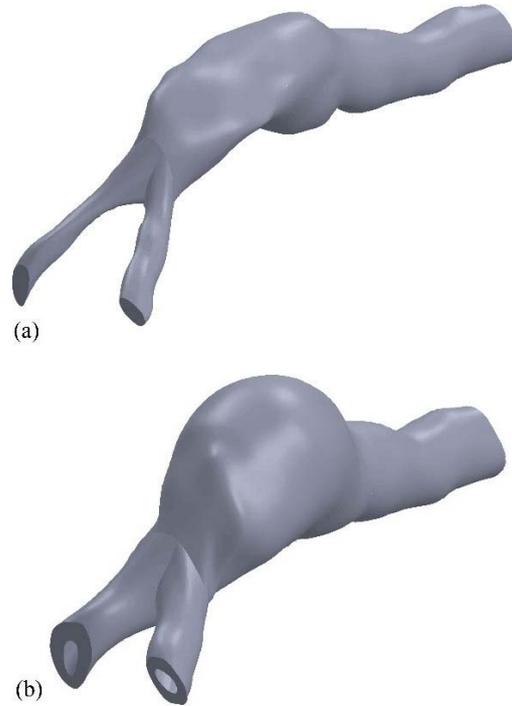

(a)

(b)

Fig. 2. AAA geometry (comprises abdominal aorta, aneurysm and common iliac arteries); (a) the fluid domain, and (b) the solid domain.

3. GOVERNING EQUATIONS AND BOUNDARY CONDITIONS

In order to simulate blood luminal flow the Navier-Stokes equations are invoked. Also, given geometrical dimensions of abdominal aorta and flow condition, blood flow remains in a laminar regime and behaves like an incompressible, Newtonian flow (Scotti and Finol, 2007). The momentum equations for the fluid domain in the Arbitrary Lagrangian-Eulerian (ALE) form can be expressed as:

$$\rho_f \frac{\partial v}{\partial t} + \rho_f \left((v - w).\nabla \right) v - \nabla.\tau_f = 0 \qquad (1)$$

In Eq. (1) ρ_f represents the fluid density. Also v is the velocity vector and w represents the moving mesh velocity vector that their subtraction imposes relative velocity in ALE formulation. Additionally τ_f is the fluid stress tensor, which is expressed as:

$$\tau_f = -p\delta_{ij} + 2\mu\varepsilon_{ij} \qquad (2)$$

where the strain rate ε_{ij} is defined as follows:

$$\varepsilon_{ij} = \frac{1}{2}\left(\nabla v + \nabla v^{T}\right) \tag{3}$$

where p is the fluid pressure, δ_{ij} is the Kronecker delta and μ is the fluid viscosity. In the current study, the blood density and viscosity are taken as $1035 kg/m^3$ and 3.5cp, respectively (Olufsen *et al.*, 2000; Perktold *et al.*, 1991; Rissland *et al.*, 2008).

In order to capture arterial wall movement due to its interaction with fluid domain, the elastodynamics equation is employed, which can be represented in Lagrangian coordinate as following:

$$\nabla.\tau_{S} + f_{S}^{B} = \rho_{S}\ddot{d}_{S} \tag{4}$$

in which τ_s is the solid stress tensor, f_s^{B} is the body force per unit volume, which is taken zero in the current study, ρ_s is the density of arterial wall that is assumed to be equal to $1200 kg/m^3$ and $\ddot{d}_s$ denotes its local acceleration.

In this study for the comparison purposes, two different models, namely, isotropic and anisotropic material models are adopted for the arterial wall. The first model is a non-linear, isotropic hyper-elastic material called Mooney-Rivlin, which its strain energy density function is expressed as:

$$\Psi = \alpha(I_1 - 3) + \gamma(I_1 - 3)^2 \tag{5}$$

where Ψ is the strain energy, I_1 is the first invariant of the Cauchy-Green deformation tensor and the values of $\alpha = 17.4 N/cm^2$ and $\gamma = 188.1 N/cm^2$ are selected based on the experimental data (Raghavan and Vorp, 2000).

For the second case, namely anisotropic material model, the exponential strain energy model proposed by Vito and Hickey (1980), along with orthotropic model, which is developed by Holzapfel *et al.* (2000) are invoked. In this model, the tissue is considered as a fiber-reinforced composite material in which collagenous components play in role of fibers in the arterial wall. Therefore, the strain energy function for AAA wall can be described as a two-term function as following:

$$\Psi = \Psi_{iso} + \Psi_{aniso} \tag{6}$$

$$\Psi_{iso} = C_1(I_1 - 3) + C_2(I_1 - 3)^2 + D_1\left(\exp\left\{D_2\left(I_1 - 3\right)\right\} - 1\right) \tag{7}$$

$$\Psi_{aniso} = \frac{k_1}{2k_2}\sum_{i=4,6}\left(\exp\left\{k_2\left(J_i - 1\right)^2\right\} - 1\right) \tag{8}$$

where

$$\begin{aligned} J_4 &= C_{ij}(n_a)_i(n_b)_j, \\ J_6 &= C_{ij}(n_a)_j(n_b)_i \end{aligned} \tag{9}$$

in which C_{ij} is the Cauchy-Green deformation tensor, n_a and n_b are directions of the fiber with respect of material axes, and they are defined by two angles β_a and β_b, respectively. The corresponding material data are taken from Rissland *et al.* (2008), which are listed in Table 2.

Table 2 Values of the material parameters for the anisotropic model

Parameter	Value
C_1 [kPa]	8.888
C_2 [kPa]	164.9
D_1 [kPa]	0.0487
D_2	53.46
k_1 [kPa]	1.886
k_2	94.75
β_a [deg]	5
β_b [deg]	265

ILT is the result of accumulation of fibrin, blood cells, platelets and lipoproteins on the inner surface of arterial walls in locations of endovascular lacerations. Most of the previous studies used a linear elasticity for the ILT (Gasser *et al.*, 2010; Papaharilaou *et al.*, 2007; Rissland *et al.*, 2008). However, in the present study following the procedure presented by Maier *et al.* (2010), ILT behavior is considered as a Neo-Hookean material model with a strain energy density function shown in Eq. (10).

$$\Psi = \phi(I_1 - 3) + \frac{\phi}{\xi}(J^{-\xi} - 1) \tag{10}$$

In Eq. (10) J is the Jacobian of the deformation tensor and the values of ϕ and ξ are based on the experimental data (ξ =4.5 and ϕ =18kPa, (Di Martino *et al.*, 1998; Gasser *et al.*, 2008; Vande Geest *et al.*, 2006)).

For analyzing hemodynamic condition in cardiovascular flow, applying appropriate boundary conditions gives more realistic and accurate outcomes. To this aim for the fluid domain, a realistic physiological waveforms for the velocity inlet with average Reynolds number of 401 and its corresponding pressure outlet are applied, which were taken from AAA in (Mills *et al.*, 1970). As shown in Fig. 3, peak systolic flow and pressure occur at t/T=0.36 and 0.45, respectively, where T is the heart beat period.

In the solid domain, for avoiding from numerical instabilities the inlet and outlet boundaries are constrained. Worth mentioning that, in the current model AAA sac is located far enough from inlet and outlet boundaries, so it reduces effects of fixed boundary assumption significantly on AAA sac displacement. Furthermore, since the arterial wall is surrounded by perivascular tissues, an external pressure of 12mmHg is applied on the outer surface

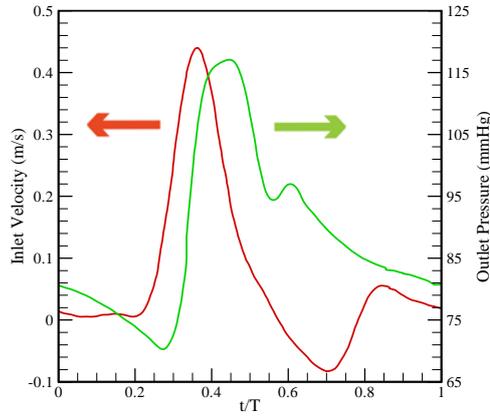of the arterial wall as intra-abdominal pressure (Hinnen *et al*., 2005).

Fig. 3. The pulsatile velocity and pressure waveforms reproduced from the study by Mills *et al*. (1970).

Finally, for coupling fluid and solid domains, continuity conditions for the displacement (Eq. (11)) and surface forces (Eq. (12)) must be applied at the fluid and solid domain interfaces. Additionally, at the interface regions the no slip boundary condition is applied for the fluid domain, which is represented in Eq. (13).

$$d_{\mathrm{F}} = d_{\mathrm{S}} \qquad (11)$$

$$n.\sigma_{\mathrm{F}} = n.\sigma_{\mathrm{S}} \qquad (12)$$

$$\dot{d}_{\mathrm{F}} = \dot{d}_{\mathrm{S}} \qquad (13)$$

where d represents the displacement, $\dot{d}$ is the local velocity, σ the stress tensor and n denotes the normal direction to the boundary surface. Also subscripts F and S denote the fluid and solid domains, respectively.

4. NUMERICAL MODELING

In order to simulate described AAA models, ADINA commercial software was employed, which is prominent software for simulating fluid-structure interaction phenomena (Raut *et al*., 2013; Rissland *et al*., 2008; Scotti *et al*., 2008; Scotti *et al*., 2005; Xenos *et al*., 2015).

In this study, the finite element procedure was invoked for solving FSI formulation of AAA. Therefore, in the fluid domain the Petrov-Galerkin method is employed for interpolating flow conditions among the elements (Bathe and Zhang, 2002), while for the solid domain the constant and bilinear functions for interpolating the pressure and displacement are used, respectively. Finally, the FSI formulations are solved by direct coupling method, which increases computational time, however helps to obtain more accurate results. During the solution process, the Newton–Raphson method is employed

for the linearization process, and discretized equations are solved by a sparse matrix solver worked based on the Gaussian elimination method. The relative tolerance for all degrees of freedom is set to 0.001. Also, for obtaining the steady-state solution of hemodynamic parameters and stress distributions of arterial wall, the results are reported after five cardiac cycles.

5. MODEL VALIDATION

To obtain an appropriate grid network, which satisfies both accuracy of the outcomes and the computationally reasonable, many different meshes were examined for the fluid and solid domains. To this aim, different sets of solid and fluid grid networks including 16 simulations were considered and finally 97873 and 359288 cellular elements in solid and fluid domains are adopted, respectively. As an instance, in Fig. 4 the variations of the maximum wall stress for three monitoring points at the time of peak systolic velocity are presented for various fluid elements, while the solid elements are kept 97873 cells. Between the last two finer grids, the results are almost similar, therefore, an intermediate grid with 359288 tetrahedral elements is chosen for the fluid domain. Similar approaches are selected for other models to obtain grid independent results. Fig. 5 demonstrates a typical tetrahedral element grid network in the fluid domain.
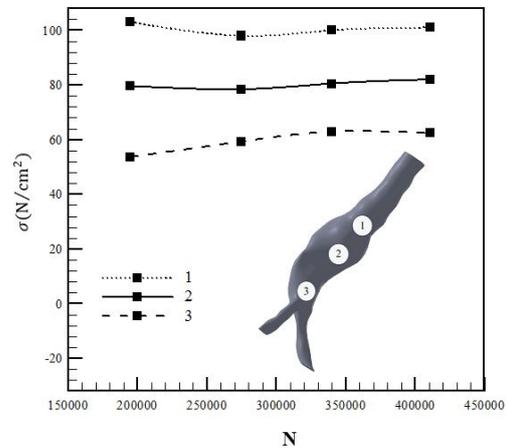

Fig. 4. Stress variations with respect to the number of grid elements for three monitoring points of fluid domain at the interface boundary with the solid domain.

6. RESULTS

Previous studies identified major effects of wall stress on wall rupture and clarified the role of wall shear stress (WSS) in genesis and growth of the aneurysm. In a pure mechanical viewpoint, rupture occurs when mechanical stresses exceed the strength of the arterial tissue. In this study, temporal variations of wall stress are considered to find the peak stress time for presenting the local

distributions of the wall stresses. These variations are also compared based on the effects of factors such as wall material model (isotropic and anisotropic) and heterogeneity of arterial wall (uniform and variable wall thickness). Moreover, local stress distributions on the outer surface of the arterial wall are depicted to clarify the situation correlated with at-risk AAAs. In order to express the effect of flow, a velocity field at the time of peak stress is depicted to qualitatively illustrate the flow motion, recirculation zones and their effects on wall stresses.

Geometric features have been demonstrated to be important predictors of peak wall stress. The role of wall thickness as a geometric factor is expected to be significant in the wall stress distributions and the rupture risk assessments. Due to limitations in the quality of medical images for estimating the thickness of arterial wall, the efforts were directed to utilize the morphological data. Following the study by Scotti *et al.* (2008), we divided the geometrical models into two categories. The first type has a uniform thickness of 1.5 mm, which is typically used in the literature (Humphrey and Holzapfel, 2012; Vorp, 2007; Vorp *et al.*, 1998). The second type with a variable thickness based on the constant wall volume assumption. In this relatively simple model, wall thickness varies inversely with diameter. Indeed, distal locations with respect of arterial centerline have smaller thickness and vice versa. Based on this model, wall thickness varies between 0.5mm and 1.5mm (Scotti *et al.*, 2008) for the cases considered here.
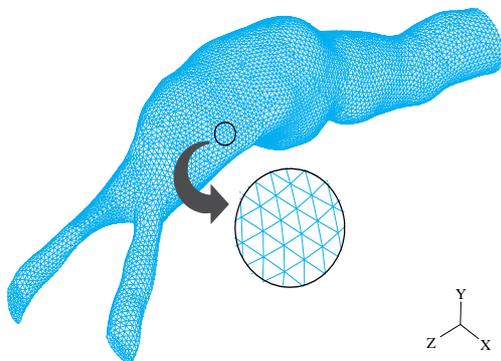

Fig. 5. Geometrical representation of tetrahedral elements grid network in the fluid domain.

Temporal variations of maximum wall stress for the UWT and VWT models are presented in Figs. 6 and 7, respectively. Results indicate that the maximum wall stress happens almost at t/T=0.41. Considering Fig. 3, this point is located between the peak systolic velocity and pressure. It implies that the accuracy of the computational solid stress (CSS) method needs essentially needs to be more scrutinized due to the velocity field effects. Scotti *et al.* (2008) compared CSS and FSI methods, and confirmed that the FSI results predict the peak stress in a different point from the peak systolic pressure.

The temporal maximum stress variations of UWT

and VWT models show similar trends for both material models in Figs. 6 and 7, respectively. In Fig. 6, the anisotropic UWT model predicts higher peak stress of about 38% as compared to the isotropic UWT model. Similarly, an increase of about 27% for the peak stress is also observed for anisotropic VWT model as compared to the isotropic model as shown in Fig. 7; yet, the stress variation trends for both material model are virtually similar.

From another perspective, temporal variations of maximum stresses for VWT models in Fig.7 closely follow similar patterns to UWT models in Fig. 6. As clearly indicated by Fig. 7, the VWT models show the increase of about 55% and 75% in peak stresses for isotropic and anisotropic material models, respectively, as compared to UWT models in Fig. 6.

Cross-sectional velocity vectors for anisotropic VWT are shown in Fig. 8 at peak stress time (t/T=0.41) in the sagittal plane. Considering Fig. 3, velocity profile at peak stress time (t/T=0.41) experiences an abrupt drop which leads to a recirculating zone near the ILT. For other models, vortices occur at almost similar locations in Fig. 8, however, with lower intensities.
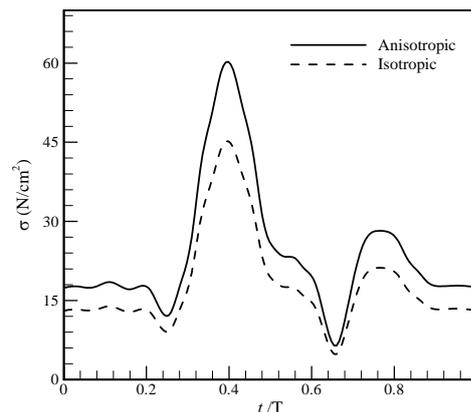

Fig. 6. Temporal variations of the maximum wall stresses for UWT models with isotropic and anisotropic materials.
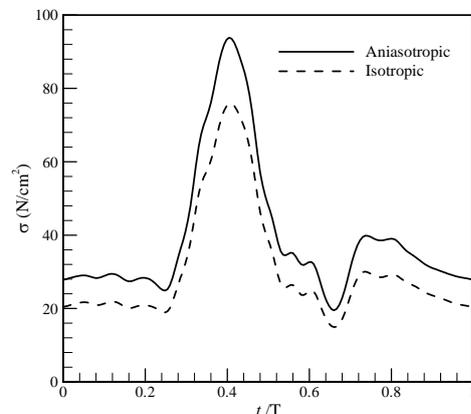

Fig. 7. Temporal variations of the maximum wall stresses for VWT models with isotropic and anisotropic materials.
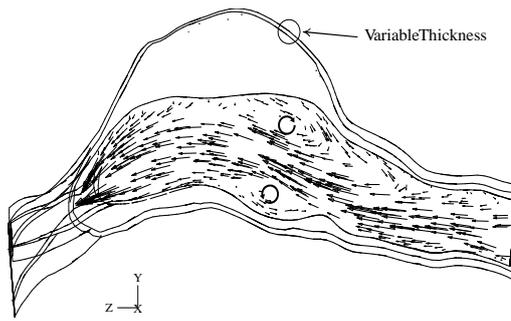
Fig. 8. Velocity vectors at (*t*/T=0.41) in a sagittal plane for anisotropic VWT model.

Spatial distributions of wall stress at outer surface if the arterial wall at peak stress time (t/T=0.41) are presented for the isotropic and anisotropic UWT models in Figs. 9a and 9b, respectively. In these figures, the anterior and posterior views of coronal plane (with 30 degrees rotation) are chosen to represent a better image of solid domain.
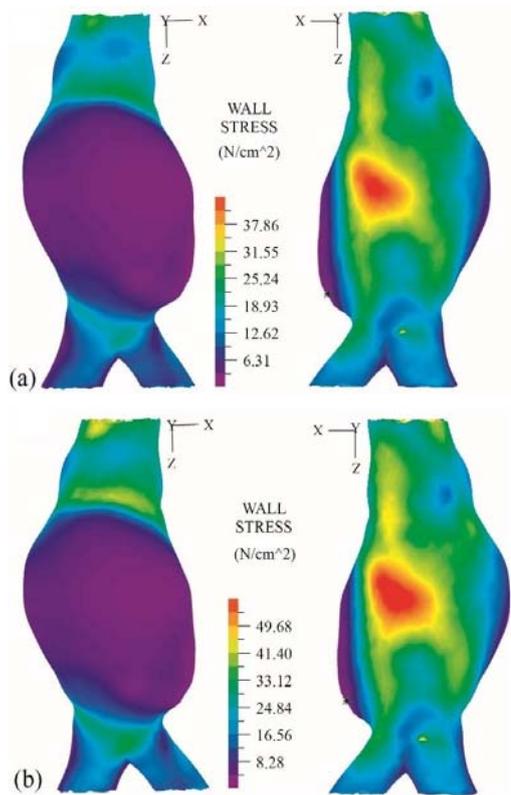

Fig. 9. Comparison of outer wall stress distributions (at *t*/T=0.41) for UWT model with (a) isotropic; and (b) anisotropic material model.

Similar stress distributions for isotropic and anisotropic VWT models are also depicted in Figs. 10a and 10b, respectively.
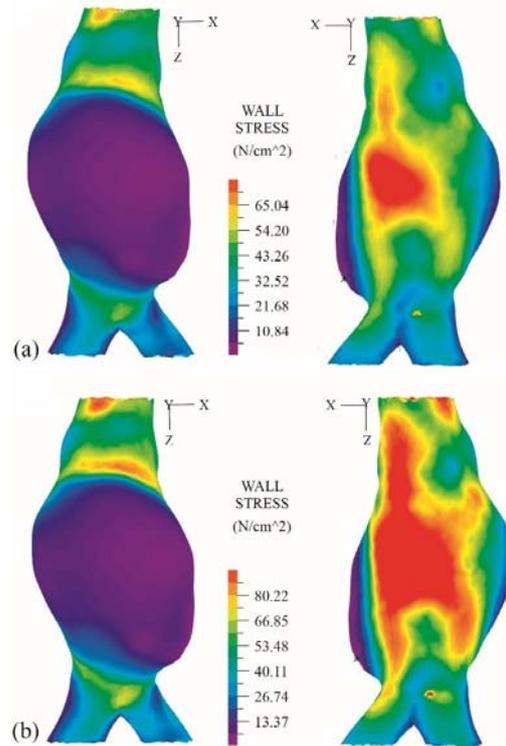

Fig. 10. Comparison of outer wall stress distributions (at *t*/T=0.41) for VWT model with (a) isotropic; and (b) anisotropic material model.

7.   DISCUSSION

A patient-specific AAA is reconstructed from CT angiographic scans and underwent to the 3D FSI analysis to assess the wall stresses based on geometric factors, specifically wall thickness and material model. One of the main purposes of this study is to analyze the wall behavior according to the isotropic and anisotropic material models. The isotropic model is a hyperelastic Mooney-Rivlin model, which is typically used in previous studies. However, the new reports of biaxial tensile tests of AAA suggest that the AAA wall behavior is more similar to anisotropic model. In this regard, an anisotropic model is employed in the FSI analysis based on orthotropic formulation and compared with the isotropic model.

According to Figs. 6 and 7, the peak stress occurs almost at the same time for all models. This result indicates that the peak stress time corresponds to the velocity and pressure profile, and is not greatly influenced by the material model and wall thickness. As previously mentioned, comparing to UWT models, the peak stresses of VWT models indicate larger values of about 55% and 75% for isotropic and anisotropic material models, respectively. Additionally, the anisotropic models predict larger peak stress values by 27% and 38% for UWT and VWT models, respectively, as compared to the isotropic models. These findings imply the major role of wall thickness on increasing wall stresses, as compared to the material models.

One of the geometrical characteristics of AAAs is the relatively sudden expansion of the artery. This expansion creates high pressure regions, which results flow separations and formation of recirculating zones. These recirculation zones create non-physiological flow conditions different from flow patterns of a healthy aorta. Flow particles like fibrin, blood cells, platelets and blood proteins may be trapped and accumulated in these regions, leading to disease progress. The flow patterns in an AAA are also important as an indicator of disorder progress. Possible locations for the formation and development of ILT are the recirculation zones where the formation of large recirculation zones is clearly depicted in Fig. 8.

Comparison between Figs. 9 and 10 indicates that both material models predict maximum and minimum of stresses at almost similar regions. Therefore, it can be concluded that the use of isotropic model represents an acceptable approximation for the stress distributions and prediction of suspected rupture locations of AAAs in the studies that require extensive processing time. The simulations with isotropic model in this study reduce the processing time by an average of 13% as compared to anisotropic models. Yet, anisotropic models describe much precise behavior of arterial wall and provide much accurate FSI analysis.

Figure 11 shows the displacements of VWT models at peak stress time (t/T=0.41) as compared to the starting time (t/T=0) for both material models. Larger wall motions are observed for the anisotropic model, which is more pronounced due to the asymmetric geometries. Numerical calculations have shown that the maximum displacements of anisotropic wall are about two times larger than the isotropic wall, and accompanied by stronger rotation around the arterial axis.
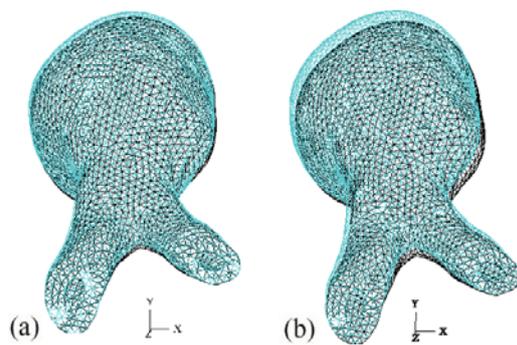

Fig. 11. Differences in wall motion between the two material models. (a) The isotropic; and (b) anisotropic models. The black and blue grids represent the beginning and peak stress times, respectively.

Referring to the stress-strain formulations of the material models, the arterial wall displacements are correlated to the wall stresses. Exponential terms in the anisotropic model (Eqs. 7 and 8) have a higher change ratio in comparison with parabolic terms in the isotropic model (Eq. 5) which is more pronounced at higher strain magnitudes resulting in the higher stresses. This clearly indicates that the employment of isotropic model underestimates the risk of rupture.

As displayed in Figs.9 and 10, the VWT models represent higher stresses for both material models as compared to the UWT models. By applying equal loads, the local thinner thickness of VWT model results in the higher rates of strains in comparison with the UWT models. Furthermore, the high stress region is broader for VWT models, which extends from below the maximum diameter to the proximal end.

Figures 9 and 10 describe that FSI analysis predicts the peak stress near the maximum AAA diameter at the posterior wall leaning to the vertebral column. This is confirmed by the autopsy reports of Darling *et al.* (1977), which indicate that approximately 80% of ruptures occur at the posterior wall. This location of peak stress confirms the current maximum diameter criterion for surgical treatment. Scotti and Finol (2007) and Rissland *et al.* (2008) reported that locations of peak stress are between the maximum diameter and the proximal/distal ends. They indicated that the peak stresses occur at the stress concentration zones, where the AAA geometries meet an abrupt change in cross-sections. This issue has been relaxed in the present study by smoothing the curvature variations of the internal surface of the realistic AAA, which minimizes the effects of stress concentrations on the locations of peak stress.

It is expected that the thinner thickness region of AAA in the anterior wall being accompanied by larger stress values; however, the presence of ILT reinforces the strength of the anterior wall by preventing the stresses induced by the recirculating flows. Therefore, the larger values of wall stresses are occurred at the posterior wall instead of the anterior wall. The lower stresses of anterior wall in Figs. 9 and 10 indicate the wall protecting effect of ILT, which is compatible with the results of the study by Rissland *et al.* (2008). However, it is notable that the inertia of ILT fluctuations causes the larger displacements near the posterior wall, which in conjunction with flow regime raise the stresses in this location. Due to the various characteristics such as geometry and flow regime for each patient, a comprehensive study based on both simulation and statistical methods seems essential. However, our study goes a step beyond the current numerical studies of AAA by considering the anisotropic VWT model. Despite the progress that has been made in the study of AAAs, there is still a need to relate these findings to clinical applications.

In future studies we will conduct a prospective and multidisciplinary study in which several patient specific AAAs will be analyzed numerically and statistically to obtain results that could be experimentally verified.

8. CONCLUSIONS

In the present study, we performed FSI simulations on a patient-specific AAA reconstructed model, which was obtained from CT angiographic scans in order to develop a more reliable indicator for prognosis rupture risk. In a comparative approach, the effects of isotropic and anisotropic material models on wall stresses for both UWT and VWT models are investigated.

Current findings demonstrate that the peak wall stress occurs between the peak systolic velocity and pressure. Analyses were done in a broad range of various wall models – in terms of isotropic/anisotropic and uniform/variable wall thickness – and it concluded that moving from isotropic UWT to anisotropic VWT, the differences become more significant, specifically at higher values of wall stress. Results confirm that the anisotropic model estimates higher stresses by 27% and 38%, for UWT and VWT models, respectively, in comparison with the isotropic model. Moreover, considering the wall thickness variability elevates wall stresses of about 55% and 75% for isotropic and anisotropic material models, respectively, comparing to the UWT model. Therefore, current outcomes underscore that the peak stresses are more influenced by wall heterogeneity comparing with material models. Also, the role of ILT as a protector of its adjacent wall is well demonstrated by lowering the stress values of anterior wall and transferring the peak wall stress to the posterior wall.

Given the importance of patient-specific geometries for the analysis of blood hemodynamics and mechanical forces, as a non-invasive diagnostic method for predicting necessity of surgical intervention, the methodology presented here can contribute significantly in predicting AAA rupture by considering more accurate and realistic parameters of AAA physiological environment.

ACKNOWLEDGEMENT

REFERENCES

Bathe, K. J. and H. Zhang (2002). A flow-condition-based interpolation finite element procedure for incompressible fluid flows. *Computers and Structures* 80(14–15), 1267-1277.

Darling, R. C., C. R. Messina, D. C. Brewster, L. W. Ottinger (1977). Autopsy study of unoperated abdominal aortic aneurysms. The case for early resection. *Circulation* 56(3 Suppl), Ii161-164.

Di Martino, E., S. Mantero, F. Inzoli, G. Melissano, D. Astore, R. Chiesa and R. Fumero (1998). Biomechanics of abdominal aortic aneurysm in the presence of endoluminal thrombus: Experimental characterisation and structural static computational analysis. *European Journal of Vascular and Endovascular Surgery* 15(4), 290-299.

Di Martino, E. S., G. Guadagni, A. Fumero, G. Ballerini, R. Spirito, P. Biglioli and A. Redaelli (2001). Fluid–structure interaction within realistic three-dimensional models of the aneurysmatic aorta as a guidance to assess the risk of rupture of the aneurysm. *Medical Engineering & Physics* 23(9), 647-655.

Di Martino, E. S. and D. A. Vorp (2003). Effect of Variation in Intraluminal Thrombus Constitutive Properties on Abdominal Aortic Aneurysm Wall Stress. *Annals of Biomedical Engineering* 31(7), 804-809.

Dorfmann, A., C. Wilson, E. S. Edgar, R. A. Peattie (2010). Evaluating patient-specific abdominal aortic aneurysm wall stress based on flow-induced loading. *Biomechanics and Modeling in Mechanobiology* 9(2), 127-139.

Doyle, B. J., A. J. Cloonan, M. T. Walsh, D. A. Vorp and T. M. McGloughlin (2010). Identification of rupture locations in patient-specific abdominal aortic aneurysms using experimental and computational techniques. *Journal of Biomechanics* 43(7), 1408-1416.

Dua, M. M. and R. L. Dalman (2010). Hemodynamic Influences on abdominal aortic aneurysm disease: Application of biomechanics to aneurysm pathophysiology. *Vascular Pharmacology* 53(1–2), 11-21.

Fillinger, M. F., S. P. Marra, M. L. Raghavan, F. E. Kennedy (2003). Prediction of rupture risk in abdominal aortic aneurysm during observation: Wall stress versus diameter. *Journal of Vascular Surgery* 37(4), 724-732.

Fillinger, M. F., M. L. Raghavan, S. P. Marra, J. L. Cronenwett, F. E. Kennedy (2002). In vivo analysis of mechanical wall stress and abdominal aortic aneurysm rupture risk. *Journal of Vascular Surgery* 36(3), 589-597.

Gasser, T. C., M. Auer, F. Labruto, J. Swedenborg and J. Roy (2010). Biomechanical Rupture Risk Assessment of Abdominal Aortic Aneurysms: Model Complexity versus Predictability of Finite Element Simulations. *European Journal of Vascular and Endovascular Surgery* 40(2), 176-185.

Gasser, T. C., G. Görgülü, M. Folkesson and J. Swedenborg (2008). Failure properties of intraluminal thrombus in abdominal aortic aneurysm under static and pulsating mechanical loads. *Journal of Vascular Surgery* 48(1), 179-188.

Grootenboer, N., J. L. Bosch, J. M. Hendriks, M. R. H. M. van Sambeek (2009). Epidemiology, Aetiology, Risk of Rupture and Treatment of Abdominal Aortic Aneurysms: Does Sex Matter? *European Journal of Vascular and*

Endovascular Surgery 38(3), 278-284.

Hinnen, J. W., O. H. J. Koning, M. J. T. Visser and H. J. Van Bockel (2005). Effect of intraluminal thrombus on pressure transmission in the abdominal aortic aneurysm. *Journal of Vascular Surgery* 42(6), 1176-1182.

Holzapfel, G. A., T. C. Gasser and R. W. Ogden (2000). A New Constitutive Framework for Arterial Wall Mechanics and a Comparative Study of Material Models. *Journal of elasticity and the physical science of solids* 61(1), 1-48.

Humphrey, J. D. and G. A. Holzapfel (2012). Mechanics, mechanobiology, and modeling of human abdominal aorta and aneurysms. *Journal of Biomechanics* 45(5), 805-814.

Kleinstreuer, C. and Z. Li (2006). Analysis and computer program for rupture-risk prediction of abdominal aortic aneurysms. *BioMedical Engineering OnLine* 5(1), 19.

Lederle , F. A., S. E. Wilson, G. R. Johnson, D. B. Reinke, F. N. Littooy, C. W. Acher, D. J. Ballard, L. M. Messina, I. L. Gordon, E. P. Chute, W. C. Krupski, S. J. Busuttil, G. W. Barone, S. Sparks, L. M. Graham, J. H. Rapp, M. S. Makaroun, G. L. Moneta, R. A. Cambria, R. G. Makhoul, D. Eton, H. J. Ansel, J. A. Freischlag and D. Bandyk (2002). Immediate Repair Compared with Surveillance of Small Abdominal Aortic Aneurysms. *New England Journal of Medicine* 346(19), 1437-1444.

Li, Z. and C. Kleinstreuer (2006). Effects of blood flow and vessel geometry on wall stress and rupture risk of abdominal aortic aneurysms. *Journal of Medical Engineering & Technology* 30(5), 283-297.

Lu, J., X. Zhou and M. L. Raghavan (2007). Inverse elastostatic stress analysis in pre-deformed biological structures: Demonstration using abdominal aortic aneurysms. *Journal of Biomechanics* 40(3), 693-696.

Maier, A., M. W. Gee, C. Reeps, J. Pongratz, H. H. Eckstein and W. A. Wall (2010). A Comparison of Diameter, Wall Stress, and Rupture Potential Index for Abdominal Aortic Aneurysm Rupture Risk Prediction. *Annals of Biomedical Engineering* 38(10), 3124-3134.

Mills, C. J., I. T. Gabe, J. H. Gault, D. T. Mason, J. J. Ross, E. Braunwald and J. P. Shillingford (1970). Pressure-flow relationships and vascular impedance in man. *Cardiovascular Research* 4(4), 405-417.

Olufsen, M. S., C. S. Peskin, W. Y. Kim, E. M. Pedersen, A. Nadim and J. Larsen (2000). Numerical Simulation and Experimental Validation of Blood Flow in Arteries with Structured-Tree Outflow Conditions. *Annals of Biomedical Engineering* 28(11), 1281-1299.

Papaharilaou, Y., J. A. Ekaterinaris, E. Manousaki and A. N. Katsamouris (2007). A decoupled

fluid structure approach for estimating wall stress in abdominal aortic aneurysms. *Journal of Biomechanics* 40(2), 367-377.

Perktold, K., R. O. Peter, M. Resch and G. Langs (1991). Pulsatile non-newtonian blood flow in three-dimensional carotid bifurcation models: a numerical study of flow phenomena under different bifurcation angles. *Journal of Biomedical Engineering* 13(6), 507-515.

Polzer, S., T. Christian Gasser, J. Bursa, R. Staffa, R. Vlachovsky, V. Man and P. Skacel (2013). Importance of material model in wall stress prediction in abdominal aortic aneurysms. *Medical Engineering and Physics* 35(9), 1282-1289.

Raghavan, M. L. and D. A. Vorp (2000). Toward a biomechanical tool to evaluate rupture potential of abdominal aortic aneurysm: identification of a finite strain constitutive model and evaluation of its applicability. *Journal of Biomechanics* 33(4), 475-482.

Raghavan, M. L., D. A. Vorp, M. P. Federle, M. S. Makaroun and M. W. Webster (2000). Wall stress distribution on three-dimensionally reconstructed models of human abdominal aortic aneurysm. *Journal of Vascular Surgery* 31(4), 760-769.

Raut, S. S., A. Jana, V. De Oliveira, S. C. Muluk and E. A. Finol (2013). The Importance of Patient-Specific Regionally Varying Wall Thickness in Abdominal Aortic Aneurysm Biomechanics. *Journal of Biomechanical Engineering* 135(8), 081010-081010-081010.

Rissland, P., Y. Alemu, S. Einav, J. Ricotta and D. Bluestein (2008). Abdominal Aortic Aneurysm Risk of Rupture: Patient-Specific FSI Simulations Using Anisotropic Model. *Journal of Biomechanical Engineering* 131(3), 031001-031001-0310 10.

Rodríguez, J. F., C. Ruiz, M. Doblaré and G. A. Holzapfel (2008). Mechanical Stresses in Abdominal Aortic Aneurysms: Influence of Diameter, Asymmetry, and Material Anisotropy. *Journal of Biomechanical Engineering* 130(2), 021023-021023-021010.

Sacks, M. S., D. A. Vorp, M. L. Raghavan, M. P. Federle and M. W. Webster (1999). In Vivo Three-Dimensional Surface Geometry of Abdominal Aortic Aneurysms. *Annals of Biomedical Engineering* 27(4), 469-479.

Scotti, C. M. and E. A. Finol (2007). Compliant biomechanics of abdominal aortic aneurysms: A fluid–structure interaction study. *Computers & Structures* 85(11–14), 1097-1113.

Scotti, C. M., J. Jimenez, S. C. Muluk and E. A. Finol (2008). Wall stress and flow dynamics in abdominal aortic aneurysms: finite element analysis vs. fluid–structure interaction. *Computer Methods in Biomechanics and Biomedical Engineering* 11(3), 301-322.

Scotti, C. M., A. D. Shkolnik, S. C. Muluk and E. A. Finol (2005). Fluid-structure interaction in abdominal aortic aneurysms: effects of asymmetry and wall thickness. *BioMedical Engineering OnLine* 4(1), 64.

Speelman, L., A. Bohra, E. M. H. Bosboom, G. W. H. Schurink, F. N. van de Vosse, M. S. Makaroun and D. A. Vorp (2006). Effects of Wall Calcifications in Patient-Specific Wall Stress Analyses of Abdominal Aortic Aneurysms. *Journal of Biomechanical Engineering* 129(1), 105-109.

Truijers, M., J. A. Pol, L. J. SchultzeKool, S. M. van Sterkenburg, M. F. Fillinger and J. D. Blankensteijn (2007). Wall Stress Analysis in Small Asymptomatic, Symptomatic and Ruptured Abdominal Aortic Aneurysms. *European Journal of Vascular and Endovascular Surgery* 33(4), 401-407.

Vande Geest, J. P., M. S. Sacks and D. A. Vorp (2006). A planar biaxial constitutive relation for the luminal layer of intra-luminal thrombus in abdominal aortic aneurysms. *Journal of Biomechanics* 39(13), 2347-2354.

Venkatasubramaniam, A. K., M. J. Fagan, T. Mehta, K. J. Mylankal, B. Ray, G. Kuhan, I. C. Chetter and P. T. McCollum (2004). A Comparative Study of Aortic Wall Stress Using Finite Element Analysis for Ruptured and Non-ruptured Abdominal Aortic Aneurysms. *European Journal of Vascular and Endovascular Surgery* 28(2), 168-176.

Vito, R. P. and J. Hickey (1980). The mechanical properties of soft tissues—II: The elastic response of arterial segments. *Journal of Biomechanics* 13(11), 951-957.

Vorp, D. A. (2007). Biomechanics of abdominal aortic aneurysm. *Journal of Biomechanics* 40(9), 1887-1902.

Vorp, D. A., M. L. Raghavan and M. W. Webster (1998). Mechanical wall stress in abdominal aortic aneurysm: Influence of diameter and asymmetry. *Journal of Vascular Surgery* 27(4), 632-639.

Wassef, M., G. R. Upchurch Jr, H. Kuivaniemi, R. W. Thompson and M. D.Tilson Iii (2007). Challenges and opportunities in abdominal aortic aneurysm research. *Journal of Vascular Surgery* 45(1), 192-198.

Wolters, B. J.B. M., M. C. M. Rutten, G. W. H. Schurink, U. Kose, J. de Hart and F. N. van de Vosse (2005). A patient-specific computational model of fluid–structure interaction in abdominal aortic aneurysms. *Medical Engineering and Physics* 27(10), 871-883.

Xenos, M., N. Labropoulos, S. Rambhia, Y. Alemu, S. Einav, A. Tassiopoulos, N. Sakalihasan and D. Bluestein (2015). Progression of Abdominal Aortic Aneurysm Towards Rupture: Refining Clinical Risk Assessment Using a Fully Coupled Fluid–Structure Interaction Method. *Annals of Biomedical Engineering* 43(1), 139-153.

Xenos, M., S. H. Rambhia, Y. Alemu, S. Einav, N. Labropoulos, A. Tassiopoulos, J. J. Ricotta and D. Bluestein (2010). Patient-Based Abdominal Aortic Aneurysm Rupture Risk Prediction with Fluid Structure Interaction Modeling. *Annals of Biomedical Engineering* 38(11), 3323-3337.